The principles of controlled DC reactor fault current limiter for battery energy storage protection

Heidary, Amir; Popov, Marjan; Moghim, Ali; Niasar, Mohamad Ghaffarian ; Lekić, Aleksandra

DOI
10.1109/TIE.2023.3257391

Publication date
2023

Document Version
Final published version

Published in
IEEE Transactions on Industrial Electronics

Citation (APA)
Heidary, A., Popov, M., Moghim, A., Niasar, M. G., & Lekić, A. (2023). The principles of controlled DC reactor fault current limiter for battery energy storage protection. *IEEE Transactions on Industrial Electronics*, *71*(2), 1525-1534. https://doi.org/10.1109/TIE.2023.3257391

The Principles of Controlled DC-Reactor Fault Current Limiter for Battery Energy Storage Protection

Amir Heidary, *Member, IEEE*, Marjan Popov, *Fellow, IEEE*, Ali Moghim, Mohamad Ghaffarian Niasar, and Aleksandra Lekić, *Senior Member, IEEE*

***Abstract*—The significance of battery energy storage systems (BESSs) technology has been growing rapidly, mostly due to the need for microgrid applications and the integration of renewables. Relevant to the importance of utilization of BESS in microgrids, the protection of the BESS during microgrid faults has become a concern too. The short circuit in a microgrid cause overcurrent for all of the integrated sources. BESS, as one of the sources in the microgrid, is heavily influenced by fault occurrence. The overcurrent can easily damage power electronic converter switches, battery management systems, and damage battery banks. Fault current limiters are appropriate protection devices that have been massively studied. In this article, we propose a controllable reactor fault current limiter (CRFCL) to protect the BESS against fault currents. The proposed CRFCL can control the fault current value supplied by BESS during a fault condition as a current regulator. It is realized by means of the operation of solid-state switches and series dc-reactor behavior. The main achievement of CRFCL is the protection of BESS against fault currents without delay. The simulations of the proposed structure are carried out in a MATLAB/Simulink platform, and they are confirmed and validated by experimental test results.**

***Index Terms*—Battery energy storage, fault current limiter (FCL), protection.**

I. Introduction

ENERGY storage systems can be connected to the dc or ac link of the ac–dc microgrid [1]. The control of energy flow in hybrid microgrids [2] and the power management strategies are two most important reasons of battery energy storage systems (BESSs) integration into the microgrids [3].

Manuscript received 16 September 2022; revised 12 December 2022; accepted 27 February 2023. Date of publication 20 March 2023; date of current version 16 August 2023. *(Corresponding author: Amir Heidary.)*

Amir Heidary, Marjan Popov, Mohamad Ghaffarian Niasar, and Aleksandra Lekić are with the Faculty of Electrical Engineering, Mathematics and Computer Science, Delft University of Technology, 2628 CD Delft, The Netherlands (e-mail: a.heidary@tudelft.nl; m.popov@tudelft.nl; m.ghaffarianniasar@tudelft.nl; a.lekic@tudelft.nl).

Ali Moghim is with the Department of Electrical Engineering, Islamic Azad University, Zanjan 58145-45156, Iran (e-mail: ali.moghim@iau.ac.ir).

Color versions of one or more figures in this article are available at https://doi.org/10.1109/TIE.2023.3257391.

Digital Object Identifier 10.1109/TIE.2023.3257391

BESSs can be used as an efficient tool to assist the integration of renewable energy source (RES) in power systems. BESS can mitigate some of the most important challenges that RES introduce in power systems [4]. In addition, energy storage is deemed necessary and important within Distributed generator (DG) renewable energy systems to ensure system stability [5].

It has been investigated that microgrid protection needs serious attention because the operation of the microgrids in both grid-connected and islanded mode depends on the existing protection strategies [6]. For microgrid protection, several protection schemes have been introduced: adaptive protection, differential protection, distance protection, voltage-based protection, and microgrid coordinated protection against faults, which proves the importance of the issue [7].

The protection of vulnerable BESS is the significant issue of the microgrid [8] to which the protection of BESS using batteries possesses two main differences compared with other applications. First, the current flow is bidirectional, both charging and discharging the batteries. Second, the impact of a short-circuit current can be very high rate of rise current (RRC) and high magnitude (because of very low internal impedance of batteries). Within Photo voltaic (PV) or wind powered applications, the fault can cause failure of battery management system, batteries, or voltage-source converter (VSC) [9], [10], [11].

The first known protection method is protection coordination method that can provide controlled microgrid and BESS protection against faults [12]. The next one is to employ fault current limiters (FCLs) as a practical solution to the mentioned issues and can protect BESS inside the microgrid [13].

Considering FCLs, the existing methods to protect microgrid and BESS are as follows.

1) Superconducting FCL technology [14]: This type of FCLs is based on superconducting resistor or reactors to protect BESS [8], [15], [16].
2) Series transformer fault current limiter (STFCL) [8] is the type of FCL where its primary side is connected in series to a power line and its secondary side is connected to a control system [17], [18], [19].
3) Saturated core fault current limiter (SCFCL), including bulky core and dc saturation circuit [20], [21].
4) DC-reactor type FCL [22] comprises of a rectifier bridge and a series dc reactor [23].

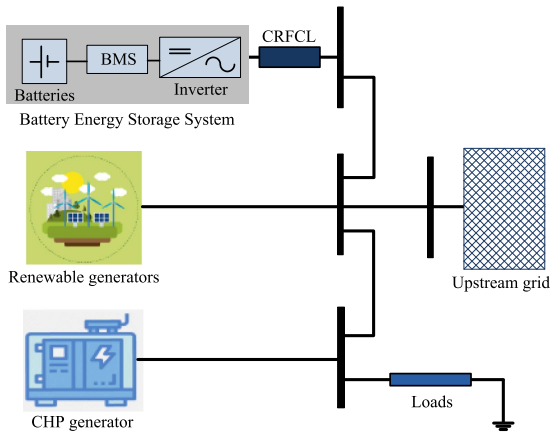

Fig. 1. BESS protection in microgrid by CRFCL.

5) Resonance-based fault current limiter (RFCL) [24], including a series reactor and capacitor bank, to protect BEES in dc microgrid [25].

In addition, the optimal placement of FCL in a microgrid is a practical method that can improve the protection of microgrid [26], [27]:

1) flux-coupled FCL for BESS protection [28];
2) Fast fault limiter and circuit breakers [8], [29], [30].

There are several urgent needs for the above-mentioned existing protection schemes that should be improved for the case of BESS protection. These are the delayed operation, high RRC, and high magnitude of fault current first peak.

In this article, a protection scheme for BESS as a vulnerable component of microgrids is proposed.This is achieved by a controlled reactor based on the power electronic, named controllable reactor fault current limiter (CRFCL). The topology of CRFCL is comprised of power electronic switches, a series dc reactor, a rectifier, and a controller. The used method of CRFCL is to provide fast fault current limitation by switching current of the dc series reactor as a controlled reactor. The main contributions and advantages of this CRFCL are given as follows:

1) designing an ultrafast FCL for BESS;
2) limiting the RRC for BESS protection;
3) limiting the first peak of fault current to BESS normal current;
4) regulating BESS current during the faulty condition.

The rest of this article is organized as follows. Section II presents the modeling of the microgrid and focuses on FCL structure. Section III discusses the system controlling strategy and associated current regulation approach. Sections IV and V report the performed analytical studies and simulation results, respectively. Section VI presents the validated results of the test setup. Finally, Section VII concludes this article.

II. CRFCL Configuration and Modeling

The proposed CRFCL is connected in series to BESS where the ac output of the power converter is connected to the microgrid bus through the CRFCL. Fig. 1 shows a four-bus microgrid that includes BESS, DGs, ac load, and an ac grid.

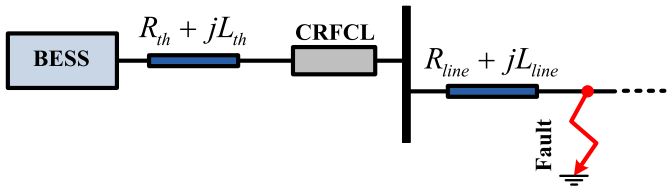

Fig. 2. BESS protection in the fault condition by CRFCL.

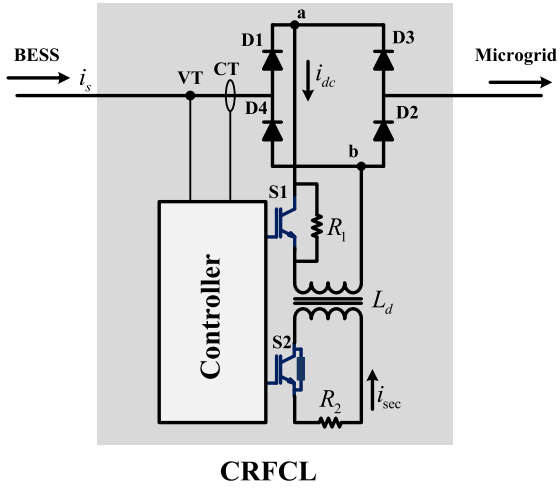

Fig. 3. Proposed CRFCL topology.

In order to analyze the operation of the proposed CRFCL, the BESS is assumed to be formed as lead-acid batteries and a single-phase VSC with a series impedance Z_s and the line impedance is shown as Z_{line}. The configuration of the fault condition is illustrated in Fig. 2.

By considering this assumption, the effects of other microgrid sections during a fault condition can be ignored, and the main focus will be on the protection of BESS against a short-circuit fault using CRFCL.

The topology of the proposed CRFCL is depicted in Fig. 3. In this structure, diodes D_1–D_4 are used as a full-bridge rectifier. The alternative input of the rectifier is connected in series to the grid and its dc part is connected to the dc reactor (L_d). The dc–dc reactor includes a main coil with a ferromagnetic core, which is magnetically coupled with a controlling secondary coil. The primary and secondary winding of dc-reactor switches using integrated gate bipolar transistor (IGBTs) S_1 and S_2. A damping resistor R_1 is placed in parallel with IGBT S_1. In addition, the controller uses the measured currents and the voltages provided by the Current transformer (CT) and the Voltage transformer (VT), respectively, and sends an operational signal to the IGBTs.

The equivalent circuit of the dc reactor and its controlled coil is shown in Fig. 4.

The equivalent representation of the transformer in Fig. 4 contains inductances L_1 and L_2 that are leakage inductances of the primary and secondary sides, respectively. Both primary and secondary winding resistances are assumed to be zero, and R_2 is the external resistance connected to the secondary transformer

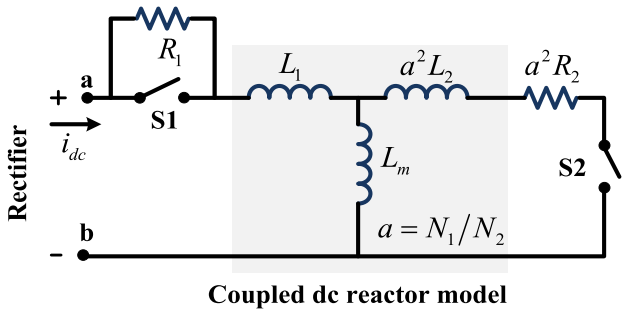

Fig. 4. Equivalent circuit of the transformer and electronic switches of the proposed CRFCL.

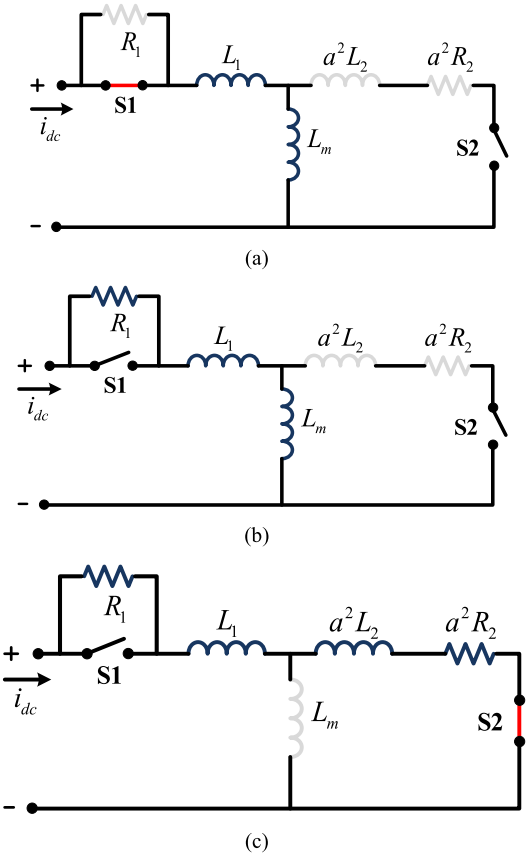

Fig. 5. Equivalent circuit of the transformer and electronic switches in the proposed CRFCL. (a) Nominal condition. (b) Faulted condition. (c) Recovery state.

side. Besides, L_m is the mutual inductance of the secondary and the primary winding. In this figure, the electronic switches are assumed to be ideal (i.e., representing short connection when closed). As indicated in Fig. 5, the states of the electronic switches determine the value of the dc reactor for different operating conditions (nominal or fault state).

In sequence one, as shown in Fig. 5(a), it is considered that the system works in a nominal condition. Thus, the switch S_1 is closed and S_2 is open. Due to the operation, the equivalent circuit is considered as a series dc reactor in series with the BESS.

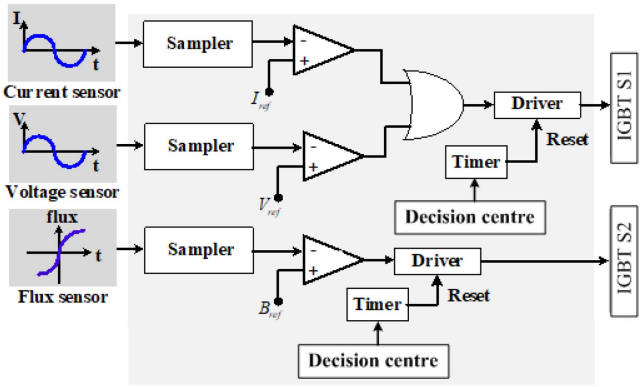

Fig. 6. Controller structure.

Because of the reactor's dc current, and its representation as the series-connected inductors, its voltage drops in steady state to a nearly zero.

In the next sequence, as illustrated in Fig. 5(b), it is considered that a fault occurred in the microgrid. The CRFCL limits the fault current by turning OFF IGBT S_1. In this state, the equivalent CRFCL circuit is R–L, which is conducted by the reactor. The resistive term is R_2 and the inductive term is given by L_1+L_m. By increasing the equivalent resistance of CRFCL and limiting effects of dc reactor, the fault current will be declined without delay.

In the third sequence, as shown in Fig. 5(c), IGBT S_2 is turned ON to recover the dc-reactor core by generating a reverse flux. This function causes an increasing value of the fault current. However, the dc reactor will be recovered to limit the fault current in the next switching period. These three sequences are carried out by using the control diagram as shown in Fig. 6.

III. Analytical Study

In this section, an analytical study of the proposed CRFCL is presented following the operational sequences. The coupled dc-reactor topology is changed by the operation of IGBTs. The logical states of the switches comprise three different circuits, connected to the full-bridge rectifier. In the first state, the equivalent circuit of the coupled dc-reactor considering the states of the electronic switches is analyzed [according to Fig. 5(a)]. Thereafter, the analysis of CRFCL is presented based on its operation in sequences two and three in the fault mode.

A. Analysis of the CRFCL (Sequence One) in Nominal State

In the first sequence denoted as a nominal state, IGBT S_1 is ON and IGBT S_2 is OFF. By applying Kirchhoff's voltage law (KVL) for the equivalent circuit, as shown in Fig. 5(a), it follows

$$-V_{\mathrm{FB}} + (L_m + L_1)\frac{di_{\mathrm{dc}}(t)}{dt} = 0. \quad (1)$$

Here, V_{FB} is a full-bridge dc voltage and i_{DC} is a dc-reactor current. The dc-reactor's current in the charging periods is formulated as a solution of the R–L circuit's ordinary differential

equation (ODE)

$$i_{\rm dc}(t) = I_{\rm in} + \left(\left(I_{\rm max} - I_{\rm in}\right)\left(1 - e^{-\alpha_c t}\right)\right) \tag{2}$$

$$\alpha_c = \frac{1}{\tau_c} = \left(\frac{R_{\rm th} + R_d + R_{\rm line} + R_{\rm load}}{L_{\rm th} + L_{\rm line} + L_1 + L_m + L_{\rm load}}\right). \tag{3}$$

Here, the direction of dc-reactor charging current is from source (BESS), including all the series impedances of the system, where $L_{\rm th}$, $L_{\rm line}$,, and $L_{\rm load}$ are the inductances of BESS, line, and load, respectively. Resistances $R_{\rm th}$, $R_{\rm line}$, R_d, and $R_{\rm load}$ are the resistances of BEES, line, diodes, and load, respectively. Value $I_{\rm max}$ is the maximum current of the power line and $I_{\rm in}$ is the initial current (i.e., current at the beginning of the time interval when the CRFCL starts operating in this state) of the dc reactor. Time constant τ_c is the ratio of the sum of all inductances and the sum of all resistances, whereas α_c is the reciprocal value of the time constant. Based on (3), it is clear that the charging time constant is relatively low.

In (4), the current of the dc reactor is considered in the discharge state when the current of the dc reactor is higher than the line current. The circuit for discharging the dc reactor is full diode bridge that works as reversed diodes. These diodes provide a very low resistance in the discharge circuit of the dc reactor. Thus, the ODE solution is given as follows:

$$i_{\rm dc}(t) = I_{\rm max} e^{-\alpha_d t} \tag{4}$$

$$\alpha_d = \frac{1}{\tau_d} = \left(\frac{R_d}{L_{\rm th} + L_{\rm line} + L_1 + L_m}\right). \tag{5}$$

Here, T_d is the time constant of the dc-reactor's current, and α_d is its reverted value. By comparing the charging and discharging time constants, it is obvious that T_c is much smaller than T_d, as illustrated in (6). The value of R_d in the discharge circuit is very small. Consequently, it is taken that the dc-reactor's current dc in the steady state has a very small variation and it becomes constant in the maximum value of line current

$$\tau_d >> \tau_c$$
$$\frac{L_{\rm th} + L_{\rm line} + L_1 + L_m}{R_d} >> \frac{L_{\rm th} + L_{\rm line} + L_1 + L_m + L_{\rm load}}{R_{\rm th} + R_d + R_{\rm line} + R_{\rm load}}. \tag{6}$$

The voltage drops of the dc reactor in steady state are almost zero [see (7)]. Furthermore, the BESS current i_s can be calculated using KVL presented in (8)

$$V_{\rm FB} = (L_m + L_1)\frac{di_{\rm dc}(t)}{dt} = 0 \tag{7}$$

$$v_s(t) = (R_{\rm th} + R_d + R_{\rm line} + R_{\rm load})\, i_s(t) + (L_{\rm th} + L_{\rm line} + L_{\rm load})\frac{di_s(t)}{dt}. \tag{8}$$

B. Analysis of the CRFCL in Fault State (Sequence Two)

After the fault occurs in the microgrid and before IGBT S_1 turns OFF, the dc-reactor's current follows (2), where α_f and $I_{\rm max}$ are calculated as follows:

$$\alpha_f = \left(\frac{R_{\rm th} + R_d + R_{\rm line} + R_{\rm fault}}{L_{\rm th} + L_{\rm line} + L_1 + L_m}\right) \tag{9}$$

$$I_{\rm max} = \left|\frac{V_s}{(R_{\rm th}+R_d+R_{\rm line}+R_{\rm fault})+j(L_{\rm th}+L_{\rm line}+L_1+L_m)}\right|. \tag{10}$$

In this sequence, the current of the source can be calculated by (7) and (8) when the value of CRFCL voltage drop is not zero anymore considering the rising rate of source current.

C. Analysis of the CRFCL in Fault State (Sequence Three)

When IGBT S_1 turns OFF, considering the operation, as shown in Fig. 5(b), the topology of the dc reactor is changed into an *R–L* circuit that can substantially control the magnitude of fault current and delay its rising nature. Accordingly, the current of the dc reactor is defined as follows:

$$i_{\rm dc}(t) = I_{\rm max} e^{-\alpha_f t} \tag{11}$$

$$\alpha_f = \left(\frac{R_1 + R_{\rm th} + R_d + R_{\rm line}}{L_{\rm th} + L_{\rm line} + L_1 + L_m}\right) \approx \left(\frac{R_1}{L_m}\right) \tag{12}$$

$$I_{\rm max} = \left|\frac{V_s}{(R_{\rm th}+R_d+R_{\rm line}+R_{\rm fault}+R_1)+j(L_{\rm th}+L_{\rm line}+L_1+L_m)}\right|. \tag{13}$$

In (12), R_1 and L_m are far higher than the other resistances and inductances in the circuit. Therefore, the other values can be neglected. In this sequence, current of the BESS can be calculated using KVL

$$V_{\rm FB}(t) = (R_1)\, i_{\rm dc}(t) + (L_m + L_1)\frac{di_{\rm dc}(t)}{dt} \tag{14}$$

$$v_s(t) = (R_{\rm th} + R_d + R_{\rm line} + R_{\rm fault})\, i_s(t) + (L_{\rm th} + L_{\rm line})\frac{di_s(t)}{dt} + v_{\rm FB}(t). \tag{15}$$

D. Analysis of the CRFCL in the Fault State (Sequence Four)

In the fourth sequence of CRFCLs operation, the IGBT S_2 will be turned ON to recover the dc-reactor core and preserve the saturation of the dc reactor. This operation is shown in Fig. 5(c). The current of the dc reactor does not pass through the high inductance magnetization branch. It mainly passes through lower parallel branches, including a series connection of the leakage inductance and resistance R_2. This operation temporarily increases the current of CRFCL until changing the controlling pulse of switches to sequence two, which follows (2), where the current of CRFCL is presented in (16), α_f is calculated as indicated in (17), and $I_{\rm max}$ is calculated as in (18)

$$i_{\rm dc}(t) = I_{\rm in} + \left(\left(I_{\rm max} - I_{\rm in}\right)\left(1 - e^{-\alpha_f t}\right)\right) \tag{16}$$

$$\alpha_f = \left(\frac{R_1 + R_2 + R_{\rm th} + R_d + R_{\rm line}}{L_{\rm th} + L_{\rm line} + L_1 + L_2}\right) \tag{17}$$

$$I_{\rm max} = \left|\frac{V_s}{(R_{\rm th}+R_d+R_{\rm line}+R_{\rm fault}+R_1+R_2)+j(L_{\rm th}+L_{\rm line}+L_1+L_2)}\right|. \tag{18}$$

In this sequence, the current of the source can be calculated by applied KVL, as shown in (15) and (19)

$$V_{\mathrm{FB}}(t) = (R_1 + R_2)\, i_{\mathrm{dc}}(t) + (L_1 + L_2)\frac{di_{\mathrm{dc}}(t)}{dt}. \tag{19}$$

E. Operation of CRFCL in Dynamic Status

To express the effect of the proposed CRFCL, in the case of power flow variation and system dynamics (because of the variation of power produced by a renewable generator or load variation), the CRFCL operation will be discussed in two operation stages. The most important assumption here is that CRFCL imposes the least amount of inductance on the system during the dynamic stages. This can mean that CRFCL does not affect the system's stability throughout the dynamic period. To study dynamic stages, two scenarios are considered as follows.

In the first scenario, it is assumed that BESS works in a steady state, and the current of BESS will be declined (first dynamic state). In this stage, the current of the dc reactor is equal to the maximum current of BESS, and then the provided dc current will be declined. It means that the stored energy of the dc reactor should be dissipated. Accordingly, an appeared voltage across the dc reactor turns ON all the diodes (series $D1$, $D4$, and series $D2$, $D3$) to freewheel the excess current of the dc reactor. During the operation, the control strategy provides a model the same as the one shown in Fig. 5(a). The free wheel current equation is

$$i_{\mathrm{dc}}(t) = I_{\max} e^{-\frac{R_d}{L_m}t}. \tag{20}$$

This operation clearly depicts that CRFCL is bypassed during the decrease of BESS current by the diodes and do not impose considerable inductance to affect the microgrid stability.

The next scenario refers to BESS current increase in dynamic mode. In this scenario, it is considered that the current of dc reactor will rise. Hence, the current of the dc reactor should rise from the initial value to the next current peak. Normally, this current increase should be limited by the dc-reactor inductance, and therefore, the system stability may be affected. To limit the effect of the inductance of CRFCL, a control strategy is applied by turning ON both S_1 and S_2. In this operation mode, the closed secondary of the dc reactor generates a reverse flux in the core. Hence, the total core flux will be the subtraction of primary and secondary winding flux, which is almost equal to zero. By using this control strategy, during this stage (dynamic of BESS increasing current), the inductance of the dc reactor can be kept to its minimum, and the system stability will not be affected. The occurrence of each dynamic state can be detected by the provided data of the current sensor. Expressions (21) and (22) describe the imposed inductance of the dc reactor during this scenario

$$\varphi_{\mathrm{total}}(t) = \varphi_1(t) - \varphi_2(t) \approx 0 \tag{21}$$

$$L_d = \frac{\varphi_1(t) - \varphi_1(t)}{i_{\mathrm{dc}}(t)} \tag{22}$$

where φ_{total} is the total value of the flux in the dc-reactor core, and φ_1 and φ_2 are the primary and secondary winding fluxes, respectively. L_d is the approximated imposed impedance of the CRFCL throughout dynamics.

TABLE I
ELECTRICAL PARAMETERS USED FOR THE SIMULATION

Categories	Symbol	Description	Value
System data	V_S	Source voltage	20kV
	Z_s	BESS equivalent resistance	0.12 Ω
	R_{line}	Line resistance	0.2 Ω
	R_f	fault resistance	0.01 Ω
	L_{line}	Line inductance	10mH
	Z_{load}	Load resistance	100 Ω
CRFCL data	L_1	primary leakage inductance	1.5 mH
	L_2	Secondary leakage inductance	1 mH
	L_m	Magnetization inductance	100 mH
	R_1	External resistance primary	10 Ω
	R_2	External resistance secondary	40 Ω

IV. CONTROLLING STRATEGY

In the proposed CRFCL, there are two IGBT switches, which change the dc-reactor topology. Initially, IGBT S_1 is turned ON and IGBT S_2 is turned OFF. An appropriate controlling method may result in a proper fault current limiting and current regulating scenario. In this approach, the measured data are BESS current and voltage realized by comparison to a digital data sampler, which can rapidly track changes using comparators C_1 and C_2. The fault occurrence causes a voltage drop and the first peak current increase. The dc reactor can limit the fault current even without a controlling system. Thus, considering the second sequence of CRFCLs operation, there is no need for a controlled pulse. Next, by rising the current and increasing the voltage drop, the controller sends a command to IGBT S_1 to turn it OFF. It causes a temporary current limitation in the third sequence; then, by increasing the core flux, which may saturate the dc reactor, the control command will turn ON IGBT S_2 to connect R_2 to the secondary winding of the dc reactor and to recover the core from saturation. This command is generated based on the operation of a magnetic sensor and a comparator C_3. Thereafter, the sequences in the fault state will repeat. This control method limits the fault current to the acceptable level, which successfully saves BESS in the fault state.

For detecting fault removal in this control structure, it is possible to reset gate signals to the initial state after adjusted time with a timer block. If the fault has been removed, the system will work in its nominal condition, and if it has not been removed, the fault limitation strategy will be repeated. The decision for timer command can be provided by a decision-making center or by the power system operators.

V. SIMULATION OF CRFCL

In this section, the simulations are run for three different scenarios. Accordingly, for the first simulation, BESS is exposed to a single line to ground fault without utilizing a protection device. In the next step, BESS uncontrolled dc reactor is employed to limit the single line to a ground fault, which is depicted in Fig. 2. For the third simulation, BESS is protected by CRFCL and a constant fault impedance is considered. Table I summarizes the electrical parameters for the simulation.

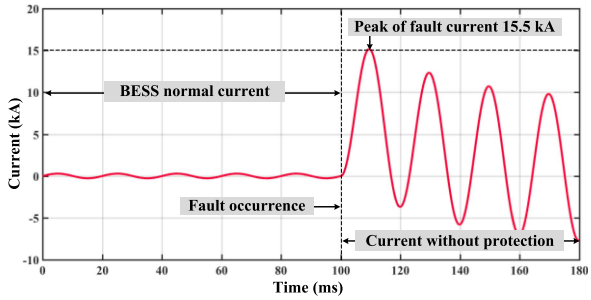

Fig. 7. BESS current during nominal and fault conditions without protection.

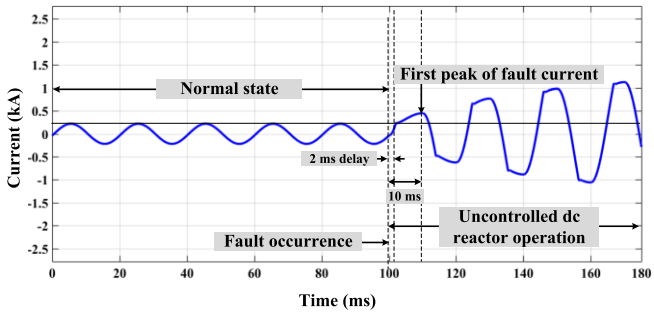

Fig. 8. BESS current during nominal and fault conditions with an uncontrolled dc reactor.

A. BESS Fault Current Without Protection

As it is obtainable from Fig. 7, theoretically, the current of BESS throughout the short-circuit fault is sharply increased to 15.5 kA as the first peak of fault current. The occurred fault creates roughly 3.9 kA/ms as RRC and an approximately permanent magnitude of 8.5 kA. This fault current can immediately damage BESS and, in reality, this fault current cannot be fed by BESS.

B. Uncontrolled DC Rector Operation

In Fig. 8, it is clearly shown that the RRC and fault current first peak are considerably limited due to the operation of the uncontrolled dc reactor. The goal of demonstration of an uncontrolled dc reactor here is to clarify the proper compensation of some delays of the protection system. This approach validates that the dc-reactor behavior successfully limits the first period of the fault current to compensate the delays of electronic-based protection devices after the fault occurs. The mentioned delays result from measurements, A/D and comparator operation, and solid-state switches operation. The total time of these delays may reach around 1–2 ms.

It is illustrated in Fig. 8 that the first peak of the fault current reaches approximately 0.4 kA, 10 ms after the fault occurrence, while the magnitude of the current after 2 ms is the same as the magnitude of the normal current. Therefore, the CRFCL control mechanism will be activated when the fault current magnitude is equal to the BESS normal current.

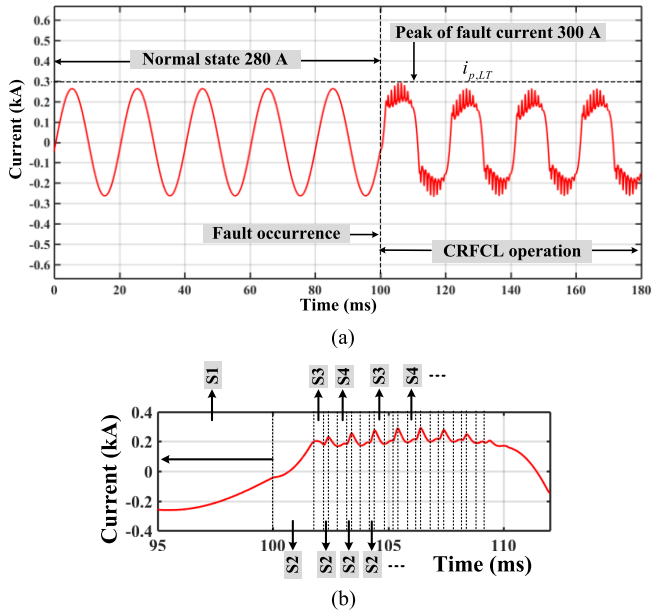

Fig. 9. (a) BESS current during a normal and a fault state with CRFCL. (b) Current closed-up view.

C. CRFCL Operation to Protect BESS

In Fig. 9(a), BESS current is depicted during the nominal and the fault condition considering the effect of CRFCL.

In this simulation example, it is shown that the average value of BESS current before and after the fault is roughly equal. It is clear that the drastically rising current stress of the BESS is entirely solved (it is 0.1 kA/ms), and the batteries meet a very small RRC. Moreover, the peak magnitude of the fault current reaches 300 A, which is in the range of the BESS nominal current. The effects of IGBTs' operation are visible by the variation in the current waveforms during the faulty states.

As seen in Fig. 9(b), S_1–S_4 refers to the switching sequences, as mentioned in Section III. Considering that S_1 is the current signal of the system during steady-state operation when the voltage drop of CRFCL is almost zero (7). At the start of operation, S_2 refers to the faulty state in which the control system does not activate the IGBT switches and the current is limited by the effects of the uncontrolled dc-reactor behavior (as it is concentrated in Fig. 8). Then, S_2, S_3, and S_4 are the switching operations during the faulty period, which is, respectively, repeated until either fault is removed or the main breaker operates.

To focus on the operational speed of the proposed CRFCL, IEEE standard C37.302-2015 [31] is considered. In this standard, $i_{p,LT}$ is the peak magnitude of the limited fault current, and T_{LT} is the time when the system reaches the first peak of fault current. These two parameters are known as the most important values that depict the performance of the studied FCL. In addition, there is a time period for which the fault has occurred but the current is the same as the system without applying an FCL. This time refers to the operational delay of the FCLs. To compare these definitions with a CRFCL operation, it is clearly

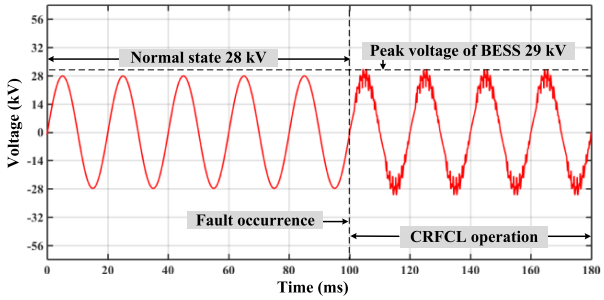

Fig. 10. BESS voltage during a normal and a fault state with CRFCL.

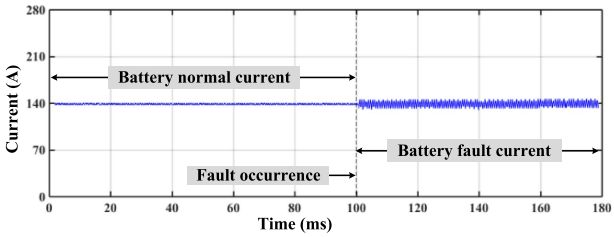

Fig. 11. BESS current during a nominal and a fault state with CRFCL.

shown that $i_{p,LT}$ is equal to the system normal current (there is no peak of fault current). Therefore, the defined time to reach the first peak of the fault current T_{LT} can be considered as zero. Moreover, the RRC of the faulty condition is not increased from the steady-state condition. So, it is obtained that CRFCL limits the fault current without operational delay (this issue is because of the effects of the uncontrolled dc-reactor nature). The magnitude of current and voltage determines the rating of the IGBT switch. Therefore, S_1 should be a package of 29 kV and 300 A switch, while on the secondary side of the dc reactor, a low-voltage switch is needed. In the current signal throughout the fault, a considerable amount of harmonics is excited. However, by taking into account that these harmonics cannot influence BESS in the faulty condition, its analysis is ignored.

In Fig. 10, the output voltage of BESS is illustrated. As shown in the simulation curve, the voltage of BESS does not fall and its average value remains almost the same value. The voltage peak value in the fault state experiences 29 kV, which is 1 kV higher than the nominal voltage. Therefore, the voltage of BESS stays nearly constant and it does not depend on the faults.

In Fig. 11, the current of the battery in the nominal state is 140 A, and in the fault state, its variation increases between approximately 130–150 A. The main consideration is that its average current is not extensively changed. The significant achievement is that the battery does not experience a high rise of a fault current or a high rate of dc current break. Therefore, this method saved both batteries and power electronic units of BESS.

In Fig. 12, control pulses of both IGBT switches are depicted during nominal and fault states.

In a normal condition switch, S_1 is ON and S_2 is OFF. On the other hand, during the faulty state, S_1 receives a pulse series with an 80% duty cycle to control the dc-reactor current, and S_2 receives a pulse with a 20% duty cycle to control the flux of the dc-reactor core.

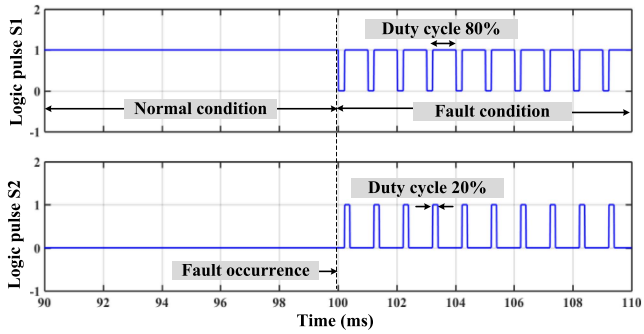

Fig. 12. Control pulse of IGBTs S_1 and S_2.

TABLE II
COMPARISON FEATURES OF CRFCL

FCL type	Operational delay	Peak of fault current	Peak of overvoltage	Required equipment
CRFCL	0	1.07 p.u.	1.03 p.u.	a DC reactor, two IGBTs
SCFCL [5]	More than 5 ms	More than 3 p.u.	More than 1.5 p.u.	AC reactor, saturable core, DC source, IGBTs, suppressor circuit
STFCL [5]	More than 1 ms	More than 3 p.u.	More than 1.5 p.u.	AC reactor, two IGBTs
RFCL [5]	More than 2 ms	More than 2 p.u.	More than 2 p.u.	AC reactor, capacitor bank, two thyristor

*Controllable reactor fault current limiter (CRFCL) *Saturated core fault current limiter (SCFCL) *Series transformer fault current limiter (STFCL) *Resonance fault current limiter (RFCL)

Considering simulation results, the performance of the presented CRFCL in comparison with three well-known FCLs is presented in Table II. The compared data demonstrate practical superiority of CRFCL.

VI. PROPOSED FCL EXPERIMENTAL TEST

The scale-down prototype is implemented considering Figs. 2 and 3 and examined by a laboratory setup. Table III provides the information on the experimented prototype. The proposed CRFCL and the laboratory setup are shown in Fig. 13.

For this purpose, a signal measurement digital oscilloscope is used, and it is connected to the setup by current and voltage sensors.

In this prototype, the dc reactor includes a toroidal ferromagnetic iron core, a copper wire primary, a copper wire secondary, and isolations. The wire cross section of the primary side is 0.5 mm^2, and with a wire the cross section of secondary winding wire is 2 mm^2. The magnetization inductance of the reactor is 100 mH. The first IGBT switch S_1 is connected in parallel with a damping resistance and is also connected to the dc-reactor primary, while the second IGBT S_2 is connected to the dc reactor and external resistor in series. IGBTs get control pulses from a digital controller.

TABLE III
PROTOTYPE EQUIPMENT DESCRIPTION

Categories	Symbol	Description	Value
Equipment data	S_1, S_2	IGBT switch	600 V, 10 A
	$D_{1\text{-}4}$	Full bridge rectifier diodes	400 V, 25 A
	BESS	Internal battery, VSC	200-400 V
	controller	A/D comparator	programmable
System data	V_S	Source voltage	380 V
	Z_s	BESS equivalent resistance	0.1 Ω
	R_{line}	Line resistance	0.2 Ω
	R_f	fault resistance	0. 1 Ω
	L_{line}	Line inductance	10mH
	Z_{load}	Load impedance	100 Ω
CRFCL data	L_1	primary leakage inductance	1.5 mH
	L_2	Secondary leakage inductance	1 mH
	L_m	Magnetization inductance	100 mH
	R_1	External resistance primary	10 Ω
	R_2	External resistance secondary	40 Ω

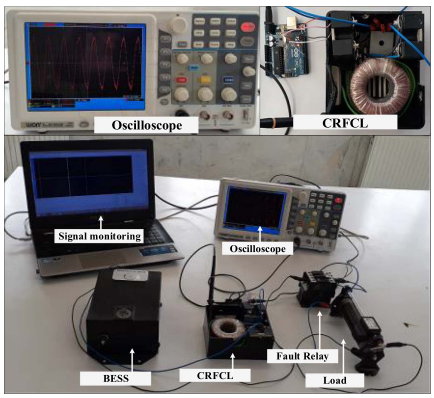

Fig. 13. Experimented laboratory prototype.

The controller consists of an A/D conversion unit, a comparator, and sensors. For this controller value of the BESS current, BESS voltage and the magnetic flux of the core are continuously measured and converted from an analog to a digital signal and compared with their reference values to provide appropriate control pulses for the IGBT switches, as explained in Section VI.

In this setup, a BESS is utilized, including a 12 V internal battery, a VSC, and a battery charging system, which are in the same package. The proposed CRFCL protects the BESS from the fault current that is connected in series with it. In addition, in this setup, the fault occurs in the line by a controllable relay. The test results are saved using a digital oscilloscope and monitored by a network connected to an online computer. The current and the voltage of BESS are illustrated in Figs. 14 and 15, respectively.

From Fig. 14, it can be seen that after fault occurrence, BESS current varies and its peak magnitude increases by nearly 0.2 A, while VSC experiences no drastic RRC. This result shows good agreement with the simulation result in Fig. 9.

In Fig. 15, BESS does not experience a sharp voltage drop throughout the fault condition; however, its peak magnitude reaches nearly 20 V. This is also in line with the simulated result in Fig. 10. Considering Fig. 16, it is obvious that the battery's dc current does not experience sharp rises or drops. The CRFCL is entirely protected by the RRC (because of the low battery impedance and the dc fault current) and rates falling current (because of the fast operation of dc breakers).

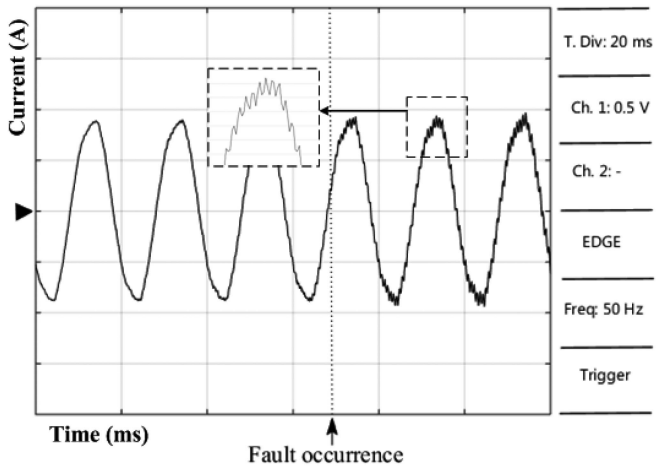

Fig. 14. BESS current in nominal and fault operation (prob X4).

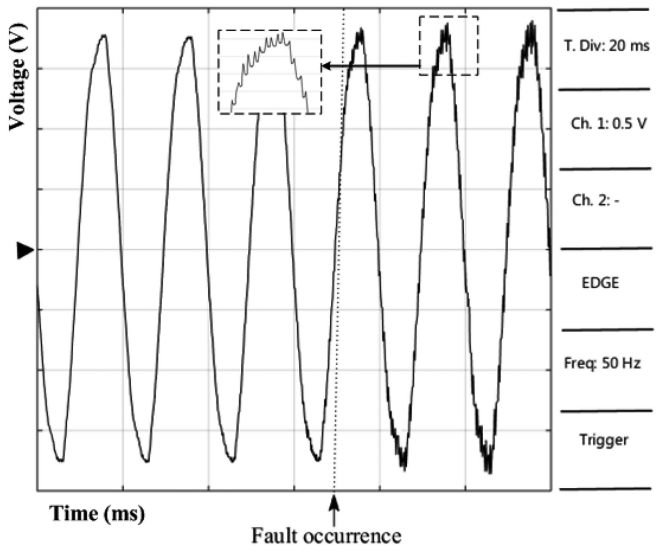

Fig. 15. BESS voltage in normal and fault operation (prob X200).

Fig. 17 illustrates the prepared pulses of control mechanism for IGBTs during the fault condition. By canceling the high rate of current change during the fault, the lifetime of the batteries can be significantly extended.

The maximum current variations, as indicated in Fig. 16, during a fault are roughly 3.6 A and 4.2 A. This result confirms the simulation results from Fig. 11. In addition, the control pulses of IGBTs S_1 and S_2 include duty cycles of almost 80% and 20%, respectively, which also confirms the simulated scenario.

VII. CONCLUSION

In this article, we presented a new topology of a CRFCL to protect a BESS for microgrids. The proposed CRFCL can limit the fault current of BESS when the fault occurs. Besides, the voltage drop does not influence BESS. Due to the operation features, BESS does not have sharp current rises or drops. A successful fault current regulation during the fault condition is entirely achieved using the proposed CRFCL. This research

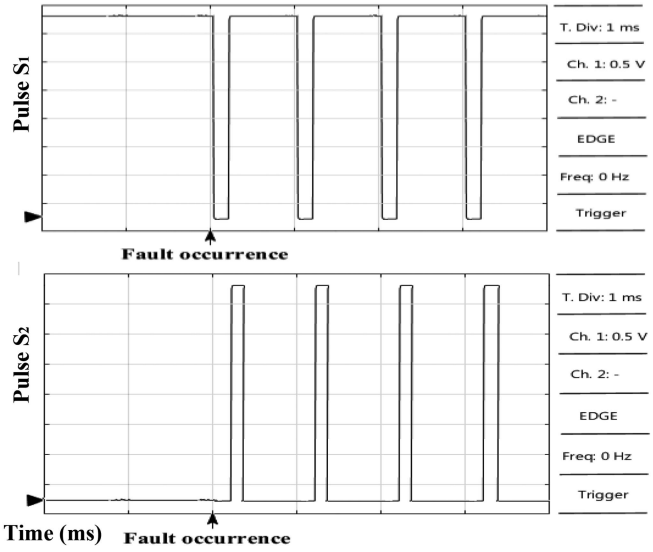

Fig. 17. IGBTs control pulses (prob X5).

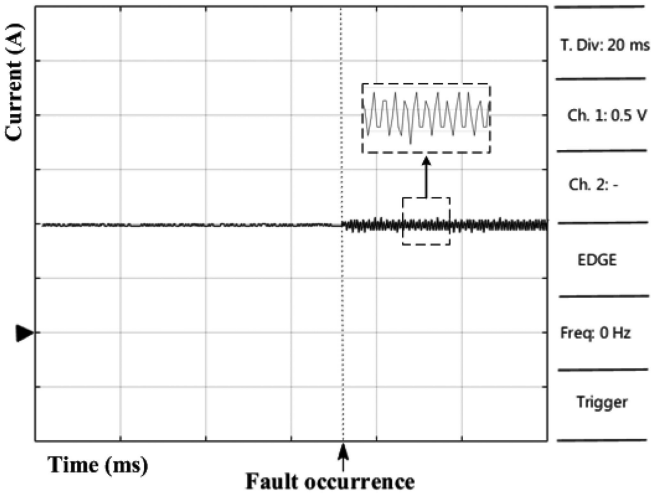

Fig. 16. Battery current in nominal and fault operation (prob X4).

introduced new principles of CRFCL operation, which were confirmed by simulation results and validated by experiments. It was proven that a BESS can be protected by CRFCL with the minimum risk of microgrid failure. The next step of this research is the implementation of real-scale CRFCL and its integration and testing upon microgrid BESS and the effects of different types of batteries will be studied.

REFERENCES

[1] X. Liu, P. Wang, and P. C. Loh, "A hybrid AC/DC microgrid and its coordination control," *IEEE Trans. Smart Grid*, vol. 2, no. 2, pp. 278–286, Jun. 2011.

[2] D. M. Rosewater, D. A. Copp, T. A. Nguyen, R. H. Byrne, and S. Santoso, "Battery energy storage models for optimal control," *IEEE Access*, vol. 7, pp. 178357–178391, 2019.

[3] A. Khademlahashy, L. Li, J. Every, and J. Zhu, "A review on protection issues in micro-grids embedded with distribution generations," in *Proc. IEEE 12th Conf. Ind. Electron. Appl.*, 2017, pp. 913–918.

[4] R. Hidalgo-León et al., "A survey of battery energy storage system (BESS), applications and environmental impacts in power systems," in *Proc. IEEE 2nd Ecuador Tech. Chapters Meeting*, 2017, pp. 1–6.

[5] M. T. Lawder et al., "Battery energy storage system (BESS) and battery management system (BMS) for grid-scale applications," *Proc. IEEE*, vol. 102, no. 6, pp. 1014–1030, Jun. 2014.

[6] X. Kang, C. E. K. Nuworklo, B. S. Tekpeti, and M. Kheshti, "Protection of micro-grid systems: A comprehensive survey," *J. Eng.*, vol. 2017, no. 13, pp. 1515–1518, 2017.

[7] A. Heidary, H. Radmanesh, K. Rouzbehi, A. Mehrizi-Sani, and G. B. Gharehpetian, "Inductive fault current limiters: A review," *Electr. Power Syst. Res.*, vol. 187, 2020, Art. no. 106499.

[8] D. M. Yehia and D.-E. A. Mansour, "Modeling and analysis of superconducting fault current limiter for system integration of battery banks," *IEEE Trans. Appl. Supercond.*, vol. 28, no. 4, Jun. 2018, Art. no. 5603006.

[9] R. M. Kamel, "Three fault ride through controllers for wind systems running in isolated micro-grid and effects of fault type on their performance: A review and comparative study," *Renewable Sustain. Energy Rev.*, vol. 37, no. 1. pp. 698–714, 2014.

[10] A. Sharma and B. K. Panigrahi, "Phase fault protection scheme for reliable operation of microgrids," *IEEE Trans. Ind. Appl.*, vol. 54, no. 3, pp. 2646–2655, May/Jun. 2018.

[11] T. S. Abdelgayed, W. G. Morsi, and T. S. Sidhu, "A new approach for fault classification in microgrids using optimal wavelet functions matching pursuit," *IEEE Trans. Smart Grid*, vol. 9, no. 5, pp. 4838–4846, Sep. 2018.

[12] K.-S. Lee, J.-M. Kim, and B.-H. Shin, "New protection coordination system according to ESS and renewable energy expansion," *CIRED-Open Access Proc. J.*, vol. 2017, no. 1, pp. 1322–1325, 2017.

[13] W.-J. Park, B. C. Sung, and J.-W. Park, "The effect of SFCL on electric power grid with wind-turbine generation system," *IEEE Trans. Appl. Supercond.*, vol. 20, no. 3, pp. 1177–1181, Jun. 2010.

[14] A. Heidary, M. Yazdani-Asrami, M. Hesami, and V. Sood, "The TRV improvement of fast circuit breakers using solid-state series superconducting reactor," *IEEE Trans. Power Del.*, to be published, doi: 10.1109/TPWRD.2022.3211778.

[15] M. E. Elshiekh, D.-E. A. Mansour, and A. M. Azmy, "Improving fault ride-through capability of DFIG-based wind turbine using superconducting fault current limiter," *IEEE Trans. Appl. Supercond.*, vol. 23, no. 3, Jun. 2013, Art. no. 5601204.

[16] A. Safaei, S. H. Hosseinian, H. A. Abyaneh, N. Fallah-Amini, and H. Hashemi-Dezaki, "Investigation of SFCL impacts on crowbar protection of DFIG based wind turbine," in *Proc. IEEE 20th Conf. Elect. Power Distrib. Netw. Conf.*, 2015, pp. 280–286.

[17] L. Chen et al., "Conceptual design and performance evaluation of a 35-kV/500-A flux-coupling-type SFCL for protection of a DFIG-based wind farm," *IEEE Trans. Appl. Supercond.*, vol. 28, no. 3, Apr. 2018, Art. no. 5200607.

[18] L. Chen, H. Chen, Z. Shu, G. Zhang, T. Xia, and L. Ren, "Comparison of inductive and resistive SFCL to robustness improvement of a VSC-HVDC system with wind plants against DC fault," *IEEE Trans. Appl. Supercond.*, vol. 26, no. 7, Oct. 2016, Art. no. 5603508.

[19] A. Heidary, H. Radmanesh, K. Rouzbehi, and J. Pou, "A DC-reactor-based solid-state fault current limiter for HVDC applications," *IEEE Trans. Power Del.*, vol. 34, no. 2, pp. 720–728, Apr. 2019.

[20] A. Heidary, K. Rouzbehi, A. Mehrizi-Sani, and V. K. Sood, "A self-activated fault current limiter for distribution network protection," *IEEE J. Emerg. Sel. Topics Power Electron.*, vol. 10, no. 4, pp. 4626–4633, Aug. 2022.

[21] F. Moriconi, F. De La Rosa, F. Darmann, A. Nelson, and L. Masur, "Development and deployment of saturated-core fault current limiters in distribution and transmission substations," *IEEE Trans. Appl. Supercond.*, vol. 21, no. 3, pp. 1288–1293, Jun. 2011.

[22] N. Shafaghatian, A. Heidary, H. Radmanesh, and K. Rouzbehi, "Microgrids interconnection to upstream AC grid using a dual-function fault current limiter and power flow controller: Principle and test results," *IET Energy Syst. Integr.*, vol. 1, no. 4, pp. 269–275, 2019.

[23] A. Heidary et al., "A multi-inductor H bridge fault current limiter," *Electronics*, vol. 8, no. 7, 2019, Art. no. 795.

[24] D. M. Yehia, D.-E. A. Mansour, and W. Yuan, "Fault ride-through enhancement of PMSG wind turbines with DC microgrids using resistive-type SFCL," *IEEE Trans. Appl. Supercond.*, vol. 28, no. 4, Jun. 2018, Art. no. 5603105.

[25] T. Ghanbari and E. Farjah, "Unidirectional fault current limiter: An efficient interface between the microgrid and main network," *IEEE Trans. Power Syst.*, vol. 28, no. 2, pp. 1591–1598, May 2013.
[26] L. Chen, Q. Chen, Z. Zhang, R. Xie, and M. Wang, "Cable fault characteristics of energy storage in DC microgrids," in *Proc. IEEE 5th Asia Conf. Power Elect. Eng.*, 2020, pp. 794–799.
[27] M. Abdolkarimzadeh, M. Nazari-Heris, M. Abapour, and M. Sabahi, "A bridge-type fault current limiter for energy management of AC/DC microgrids," *IEEE Trans. Power Electron.*, vol. 32, no. 12, pp. 9043–9050, Dec. 2017.
[28] W.-S. Moon, J.-N. Won, J.-S. Huh, and J.-C. Kim, "A study on the application of a superconducting fault current limiter for energy storage protection in a power distribution system," *IEEE Trans. Appl. Supercond.*, vol. 23, no. 3, Jun. 2013, Art. no. 5603404.
[29] W. Guo, L. Xiao, and S. Dai, "Fault current limiter-battery energy storage system for the doubly-fed induction generator: Analysis and experimental verification," *IET Gener., Transmiss. Distrib.*, vol. 10, no. 3, pp. 653–660, 2016.
[30] L. Chen, H. Chen, J. Yang, Y. Tang, and L. H. Koh, "Optimal allocation of flux-coupling-type SFCLs for a micro-grid with wind-PV hybrid generation and battery energy storage," in *Proc. IEEE Asian Conf. Energy, Power Transp. Electrific.*, 2016, pp. 1–5.
[31] *IEEE Guide for Fault Current Limiter (FCL) Testing of FCLs Rated Above 1000 V AC*, IEEE Standard C37.302-2015, pp. 1–64, May 2016.

Amir Heidary (Member, IEEE) was born in Tabriz, Iran, in 1987. He received the B.Sc. and M.Sc. degrees in electrical power system engineering from the Department of Electrical Engineering, Islamic Azad University, Zanjan, Iran, in 2009 and 2020, respectively. He is currently working toward the Ph.D. degree in Smart grids protection with the Delft University of Technology, Delft, The Netherlands.

He worked with Eleprotect Company as a researcher of electrical applications from 2012 to 2017. His research has been published in books, journal articles, and several patents. His invention was awarded to the Iranian elite foundation in 2014. His main research interest include future power system protection, magnetic-based power applications, smart grids, and fast transients.

Marjan Popov (Fellow, IEEE) received the Ph.D. degree in electrical power engineering from the Delft University of Technology, Delft, The Netherlands, in 2002.

He is a Professor of power system protection with the Delft University of Technology. He is also a Chevening Alumnus and, in 1997, he was an Academic Visitor with the University of Liverpool, Liverpool, U.K., working in the Arc Research Group on modeling SF6 circuit breakers. His major fields of interest are future power systems, large-scale power system transients, intelligent protection for future power systems, and wide-area monitoring and protection.

Prof. Popov was a recipient of the prestigious Dutch Hidde Nijland Prize for extraordinary research achievements in 2010, the IEEE PES Prize Paper Award, and IEEE Switchgear Committee Award in 2011. He is an Associate Editor for *Elsevier's International Journal of Electrical Power and Energy Systems*. In 2017, together with the Dutch utilities TenneT, Alliander, and Stedin, he founded the Dutch Power System Protection Centre to promote research and education in power system protection. He is a member of Cigre and actively participated in WG C4.502 and WG A2/C4.39.

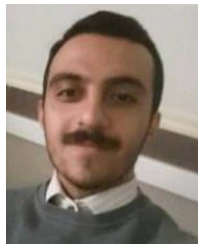

Ali Moghim was born in Zanjan, Iran, in 1998. He received the B.Sc. degree from Alghadir University, Zanjan, Iran, in 2019.

He is currently with Eleprotect Company as a Technician of electrical applications. He is interested in power system protection, renewable energy resources, smart grids, and fast transients.

Mohamad Ghaffarian Niasar was born in Tehran, Iran, in 1984. He received the M.Sc. degree in electrical power engineering from the Sharif University of Technology, Tehran, Iran, in 2008, and the Ph.D. degree in electrical engineering from the KTH Royal Institute of Technology, Stockholm, Sweden, in 2015.

He is currently an Assistant Professor with High Voltage Technology Group, Technical University of Delft, Delft, The Netherlands. His main research interests include aging of electrical insulation, HVdc insulation system, partial discharges, high-voltage power electronics, high-frequency power transformers, power cables, and FEM modeling.

Aleksandra Lekić (Senior Member, IEEE) received the B.S., M.S., and Ph.D. degrees in electrical engineering from the School of Electrical Engineering, University of Belgrade, Belgrade, Serbia, in 2012, 2013, and 2017, respectively.

Between 2012 and 2018, she was a Teaching Assistant with the School of Electrical Engineering, University of Belgrade, and an Assistant Professor from 2018 to 2019. In 2019, she worked as a Postdoctoral Researcher with the Department of Electrical Engineering (ESAT), KU Leuven, and the Institute of EnergyVille, Genk, Belgium. Since January 2020, he has been an Assistant Professor with the Faculty of Electrical Engineering, Mathematics and Computer Science, TU Delft, in the Group Intelligent Electrical Power Grids.